Electronic Structure of the 1D Conductor $K_{0.3}MoO_3$ studied using Resonant Inelastic X-ray Scattering and Soft X-ray Emission Spectroscopy

T. Learmonth,[1] P.-A. Glans,[1] C. McGuinness,[2] L. Plucinski,[1] Y. Zhang[1], J.-H. Guo[3], M. Greenblatt,[4] and K. E. Smith.[1]*

[1]Department of Physics, Boston University, 590 Commonwealth Ave., Boston, MA 02215

[2]School of Physics, Trinity College Dublin, Dublin 2, Ireland

[3]Advanced Light Source, Lawrence Berkeley Laboratory, Berkeley, CA 94720

[4]Department of Chemistry and Chemical Biology, Rutgers University, Piscataway, NJ 08854

Abstract:

The electronic structure of the quasi-one dimensional conductor $K_{0.3}MoO_3$ has been measured using high resolution resonant inelastic x-ray scattering and x-ray absorption spectroscopy. The data is compared to that from the related two dimensional insulator α-MoO_3. Scattering features are observed from both oxides that are explained in terms of the band momentum selectivity of the scattering process, allowing a comparison of the scattering data to recent band structure calculations.

PACS: 78.70.En

Synchrotron radiation excited resonant inelastic x-ray scattering (RIXS) and soft x-ray emission spectroscopy (XES) are emerging as important probes of electronic structure in complex materials. XES allows the local, element- and site-specific partial density of states (PDOS) to be measured for valence band states, while RIXS measures low energy valence excitations with the same element and site specificity.[1,2] An interesting issue in the application of these spectroscopies is their sensitivity to the dimensionality of the sample. We report here an exploration of dimensional effects in soft x-ray emission and scattering from the prototypical low dimensional transition metal oxide $K_{0.3}MoO_3$ ("blue bronze"). X-rays scattered at the O *K*-edge were found to be sensitive to the band momentum, **k.** This is unexpected since the strong quasi-one dimensionality in $K_{0.3}MoO_3$ would favor a more localized interaction,[3] and the strong electron - phonon coupling associated with the Peierls transition observed in $K_{0.3}MoO_3$ may serve to scatter the intermediate state.[4] Our results provide new insight on the electronic structure of molybdenum oxide bronzes.

Quasi-one dimensional (1D) transition metal oxides have been studied for many years since they exhibit some of the most complex electronic behavior in solids. Strong electron-electron and electron-phonon interactions lead to phenomena such as charge density waves, superconductivity, periodic lattice distortions, and Peierls transitions.[5,6] $K_{0.3}MoO_3$ is a member of a large class of quasi-low dimensional layered materials, the Mo oxide bronzes,[7] and displays a strongly anisotropic electronic structure.[4,6] The parent compound α-MoO_3 has a related crystal structure, but is a quasi-two dimensional (2D) insulator. Despite the enduring interest in these materials, there have been few measurements of their electronic structure using RIXS or resonant soft x-ray emission spectroscopy XES.[8] RIXS can be used, under the proper circumstances, to probe the **k** resolved band structure of solids.[9-11] The mechanism that provides **k** selectivity is

not direct, as in angle-resolved photoemission (ARPES), but dependent on the properties in **k** space of the intermediate and final RIXS states. As a result, the subset of the Brillouin zone represented in a particular RIXS spectrum can be rather complex. There are also exceptions to band momentum conservation that are not simple to predict. For instance, in the graphite C *K* edge RIXS results from Carlisle *et al.*, there is strong **k** selectivity at excitation energies close to the C *K*-edge, but the band features appear on a background that roughly resembles the non-resonant (fluorescent) C *K* edge x-ray emission spectrum.[11] The origin of the background lies in the interaction of the intermediate RIXS state with the rest of the system.[2,9,12] The decay of the intermediate state via an interaction (prior to the decay of the core hole) alters the momentum of the RIXS state, destroying the momentum selectivity of the process. This gives rise to a portion of the RIXS spectrum that is not **k**-selective and the relative magnitude of this background is a point of some contention.[13] Despite the lack of ability to predict precisely the background intensity in **k**-selective RIXS, the intermediate state and core hole lifetimes together may provide some indication of the expected scale. If the intermediate state is much longer lived than the core hole, then the RIXS process is "coherent" and **k**-selective.[9] If the intermediate state is approximated as infinitely long lived compared to the core hole, the background (**k**-unselective) intensity can be thought of as the degree to which this approximation does not hold. Then assuming this condition on relative lifetimes is met, in order to observe **k**-selective RIXS in a broad band solid, it is also necessary for the intermediate and final states to disperse with **k** on a scale larger than the experimental resolution. In materials with band-like unoccupied states, the unoccupied states at a specific energy might span only a subset of the Brillouin zone. So RIXS experiments may produce **k**-selective features if the incident photon energy resolution is small enough such that the set of accessed RIXS intermediate states does not span the entire Brillouin

zone. In this case a portion of each RIXS spectrum will be representative of the local occupied partial density of states (PDOS) only from the region of the Brillouin zone selected by the RIXS intermediate state.

We have used O *K*-edge RIXS, XES and x-ray absorption spectroscopy (XAS) to measure the O *2p*-derived valence and conduction band electronic structure in $K_{0.3}MoO_3$. We compare our results to those from the 2D band insulator α-MoO_3. Measurements were performed at beamline 7.0.1 at the Advanced Light Source (ALS), Lawrence Berkeley National Laboratory, and at beamline X1B at the National Synchrotron Light Source, at Brookhaven National Laboratory. Both are undulator beamlines equipped with spherical grating monochromators. X-ray absorption spectra were recorded in either total electron yield (TEY) mode for conducting $K_{0.3}MoO_3$, measured via the sample drain current, or in total fluorescent yield (TFY) mode for insulating α-MoO, measured using a Si diode. XAS energy resolution at the O *K*-edge was 0.2 eV. The XAS energy scale was calibrated at the ALS using the O *K*-edge x-ray absorption structure of NiO.[14] RIXS and XES measurements were made in ultra-high vacuum using a Nordgren type spherical grating x-ray spectrometer.[15] The O *K*-edge emission was calibrated to metallic Zn $L_{\forall 1,2}$ and $L_{\exists 1}$ emission lines in second order. RIXS and XES measurements were performed with a spectrometer resolution of 0.4 eV and a monochromator resolution of 0.4eV. RIXS/XES measurements were made with the incident photon polarization vector in two modes: either almost parallel to the quasi-one dimensional **b** crystal axis, or with the incident photon polarization vector almost perpendicular to the **b** axis. (The crystal axes are discussed in more detail below.) The detector is placed 90< from the incident photon beam, with the incident photon polarization vector inside the plane of scattering. Thus we only detect

emitted photons with a polarization perpendicular to that of the incident photons. We are unable to measure RIXS with the incident photon polarization vector exactly parallel to either the sample surface or the sample surface normal, but must move approximately 15< away from the desired axis to allow x-rays to both enter and exit the sample in the appropriate directions. All of the RIXS/XES spectra are normalized to the main peak maximum, so all noted intensity changes are relative to the peak of the observed emission at 526.1 eV. The $K_{0.3}MoO_3$ samples were cleaved in a N_2 atmosphere immediately prior to introduction to vacuum, with care taken to prevent exposure to air. The α-MoO_3 sample was scraped with a razor blade immediately before introduction to vacuum to expose a fresh surface. To minimize photon stimulated desorption and any other radiation damage,[16,17] the sample was rastered during measurements to expose a fresh surface to the x-ray beam approximately every 30 minutes.

Figure 1 presents the crystal structures of $K_{0.3}MoO_3$ and α-MoO_3. The $K_{0.3}MoO_3$ unit cell is monoclinic, with clusters of chains of MoO_6 octahedra along the **b** axis. The chains of octahedra are joined via corner sharing, forming sheets along the [102] direction which are separated by planes of potassium atoms.[18] $K_{0.3}MoO_3$ samples cleave along these potassium planes, exposing the $[\bar{2}01]$ surface. Here the direction is specified by its real space lattice vector, and the surface by its Miller index. In contrast, α-MoO_3 has an orthorhombic unit cell, with pairs of chains of octahedra along the **b** axis. The chains share corners with neighboring chains along the **c** axis, with no shared sites along the **a** axis.[7] Thus it is tempting to consider the α-MoO_3 **b**, **c**, and **a** axes similar to the $K_{0.3}MoO_3$ **b**, [102], and $[\bar{2}01]$ axes. In this sense, both samples cleave in a similar way, with α-MoO_3 exposing the plane normal to **a**.

XAS and XES results from $K_{0.3}MoO_3$ where $\mathbf{E}_{in} \parallel \mathbf{b}$ and $\mathbf{E}_{in} \parallel [102]$, taken at near normal incidence, are presented in the top panel of Fig. 2. As reported earlier,[8] only small differences in the emission spectra between the two crystal orientations are observed. The XES spectra are relatively broad, resolving primarily only a cluster of σ and π states at 522.5 eV and 525.5 eV, respectively. The XES spectra are recorded for excitation energies well above the O *K*-edge threshold, and represent the O *2p* partial density of states. In both orientations, the width of the emission band is 6 eV, which corresponds well to both XPS measurements,[19,20] and calculations of valence band width.[21] In the $\mathbf{E}_{in} \parallel [102]$ orientation, there is an increase in spectral weight, relative to $\mathbf{E}_{in} \parallel \mathbf{b}$, above the main π peak at ~ 528 eV. This is the energy region near E_F, and is dominated by states primarily of Mo *4d* character, as previous observed using photoemission spectroscopy.[4,17,20] These states are visible in the O *K*-edge XES spectra due to Mo *4d* - O *2p* hybridization. They arise due to Mo-O π bonding along the [102] axis, where the bonding O *2p* orbital is parallel to the **b** axis, and thus the states have the strongest projection along the **b** axis.[21] With $\mathbf{E}_{in} \parallel \mathbf{b}$ in our 90< measurement geometry, we only detect emission which has a polarization vector perpendicular to **b**, and thus dipole emission from these states is most easily observed with $\mathbf{E}_{in} \parallel [102]$. Such symmetry selection in XES arising from different measurement geometries with respect to bond directions is only to be expected in crystalline systems.[22] The XAS results from $K_{0.3}MoO_3$ are also similar between the two orientations. The π* peak and σ* peaks appear at 530.8 eV and 534.5 eV, respectively, in both cases. A change in relative intensity of the π* peak and σ* peaks is seen between the two sample orientations, and agrees with previously published results.[8,23] The shape of the B* peak, especially on the low energy side, is nearly identical in the two orientations. This similarity, along with the results of a DFT

calculation of the low lying unoccupied states,[21] suggests that at least the lower energy side of the peak originates from the same band in both orientations. The bottom panel of Fig. 2 shows the XES and XAS results for insulating α-MoO_3. The XES from α-MoO_3, again obtained well above the O *K*-edge threshold, is nearly identical to that obtained from $K_{0.3}MoO_3$ (top panel). The only substantive difference is a shift in absolute energy of the main peak of the emission spectrum by approximately 0.3 eV. The O *K*-edge XAS spectrum from α-MoO_3 is, however, quite different from that obtained from $K_{0.3}MoO_3$. The π^* peak at 530 eV is about 0.8 eV lower in energy than the $K_{0.3}MoO_3$ π^* peak, and is about 0.5 eV broader. The Φ_1^* and Φ^* peaks at 531.9 and 534.1 eV are both easily visible in α-MoO_3, while in $K_{0.3}MoO_3$ the Φ_1^* peak is suppressed and visible only as a shoulder. The B - B* separation appears to be approximately 1 eV less in α-MoO_3 than in $K_{0.3}MoO_3$. We note that while our measurements were made at room temperature, our XAS results are similar to recent XANES measurements made at 140 K, which is below the Peierls transition temperature of 180 K.[23]

Figure 3 presents RIXS spectra excited near the O *K*-edge threshold the $\mathbf{E}_{in} \parallel \mathbf{b}$ orientation, (bottom panel) and the associated XAS spectrum from $K_{0.3}MoO_3$ (top panel). RIXS spectra recorded in our two experimental orientations are markedly different. The RIXS spectra recorded in the $\mathbf{E}_{in} \parallel [102]$ geometry strongly resemble the XES spectra shown in Fig. 2, and display little dependence on the excitation energy and are not presented here. However, the spectra presented in Fig. 3 collected in the $\mathbf{E}_{in} \parallel \mathbf{b}$ orientation are quite different than the XES spectrum in Fig. 2. In this orientation there are two well resolved features, at 525 eV and 526.1 eV, (labeled *i* and *ii*, respectively) in spectra A through C, where the letters correspond to the excitation energies marked in the XAS spectrum (top panel). The emission energies of

features *i* and *ii* do not track with changes in excitation energy. This suggests that these features do not originate from localized excitations, and that a band interpretation may be appropriate.[12] Also visible in spectra A through C in Fig. 3 is a reduction in spectral weight (relative to spectra D and E) on both the high energy edge of the main emission feature, and the low energy side below about 524 eV. For spectrum D and higher excitation energies the XES spectrum resembles the PDOS, as in Fig. 2.

Figure 4 presents the equivalent XAS and RIXS spectra from α-MoO_3, with the **b** axis aligned to the incident x-ray polarization vector. The results are quite similar to those obtained from $K_{0.3}MoO_3$. There are two primary RIXS features, and strong suppression of spectral weight outside those features. However, feature *i* slowly shifts with increasing excitation energy toward higher emission energy while feature *ii* broadens considerably. This shift in emission energy observed in α-MoO_3, along with the suppression of spectral weight, points to **k**-selectivity in the RIXS spectra. Given the similarity between the $K_{0.3}MoO_3$ and α-MoO_3 RIXS spectra, it is tempting to ascribe a similar origin to the common spectral features, although we cannot clearly resolve a shift in feature *i* in the $K_{0.3}MoO_3$ RIXS spectra. (Note that a comprehensive report on the electronic structure of α-MoO_3 studied using XES and RIXS can be found elsewhere.[24])

Figure 5 shows the position of features *i* and *ii* from $K_{0.3}MoO_3$ and α-MoO_3 for each excitation energy in which they are observed. In α-MoO_3, feature *i* shifts to higher energy by 0.3 eV over a range of 1.6 eV in excitation energy. The calculated bandwidth of the lowest energy unoccupied band is ~ 1.5 eV,[25] so it is likely that the **k**-selectivity in α-MoO_3 is tied to excitations into the lowest unoccupied band. On the other hand, the calculated bandwidth of the lowest unoccupied band in $K_{0.3}MoO_3$ is ~ 0.3 eV.[21] Our experimental resolution places a lower

bound greater than 0.4 eV on the lowest unoccupied bandwidth, since at each **k**-selective excitation energy we must probe less than the entire band. A stronger lower bound would apparently be placed on the bandwidth by the 1.3 eV excitation energy range in which **k**-selectivity is observed. However, it is also possible for **k**-selectivity to persist through more than one unoccupied band, the hallmark of which is a change in the direction of the shift in energy of the **k**-selective RIXS features.[11] For $K_{0.3}MoO_3$, we cannot be sure of the number of unoccupied bands involved in the observed **k**-selectivity, since a change in the direction of any shift in energy of either feature *i* or *ii* is not measurable. Thus the lower bound placed by the experimental resolution on the lowest unoccupied band in $K_{0.3}MoO_3$ appears to be the strongest one definitively supported by observation.

Referring to the XAS spectrum collected in the $\mathbf{E}_{in} \parallel \mathbf{b}$ orientation (see Fig. 3), it is apparent that the 1.3 eV range in which the **k**-selectivity is observed corresponds to excitations into the π* band. Thus the dispersive unoccupied states that provide the **k**-selectivity originate in π* bonds with O *2p* components that lie parallel to the **b** crystal axis. The origin of the O *K*-edge RIXS features themselves, however, are less clearly identifiable. Feature *ii*, at 526.1 eV, is firmly within the π bands marked in Fig. 2. Thus the bonds responsible for the feature are π bonds where the O *2p* component of the bond lies in the plane perpendicular to the **b** axis. At 525 eV, feature *i* may fall in the same category, but it is not as clear from the emission in Fig. 3 where the division between the π and σ bands lie, or indeed if there really is a strict division at all. If feature *i* does correspond to the π band like feature *ii*, then it also originates in a π bond where the oxygen *2p* component is perpendicular to the **b** crystal axis. But if it corresponds to the σ band, then it originates in a σ bond perpendicular to the **b** crystal axis. As the prominent

peaks in the RIXS spectra must arise from the oxygen *2p* projection of the PDOS from bands that are essentially dispersionless in the direction perpendicular to the **b** axis, we may expect that the Mo-O π bonding is contained in the plane perpendicular to the one-dimensional **b** axis.

The widths of the **k**-selective features are also of interest. Feature *i* has a width that is difficult to measure, due to uncertainties about the shape of the background on which it appears. The width of feature *ii* is simpler to estimate, largely because it is less influenced by the background. Fitting a Gaussian peak to feature *ii* in the lowest energy spectrum from each material, the widths are 0.75 and 1.1 eV in α-MoO_3 and $K_{0.3}MoO_3$, respectively. This difference in width could originate in a number of ways. Perhaps most obvious is a difference in the dispersion of the unoccupied band probed in each material during the RIXS process. If, as calculations suggest, the lowest unoccupied band in α-MoO_3 disperses more strongly than the lowest unoccupied band in $K_{0.3}MoO_3$,[21,26] then each **k**-selective RIXS spectrum in α-MoO_3 probes a smaller section of the Brillioun zone than each **k**-selective RIXS spectrum in $K_{0.3}MoO_3$. This picture may also explain the larger energy shift of feature *i* in α-MoO_3 than in $K_{0.3}MoO_3$. Alternatively, it is also possible that the larger width measured in $K_{0.3}MoO_3$ is at least in part due to greater width of the occupied band corresponding to feature *ii*. Thirdly, the difference in width could be the effect of intermediate state scattering. In α-MoO_3, the 3 eV band gap suppresses multielectron scattering in the intermediate state.[9] In $K_{0.3}MoO_3$, there is no band gap, and although the density of states at E_F in $K_{0.3}MoO_3$ is small, multielectron scattering may play a role. Lastly, the difference in peak width could be due to the existence of a shallow exciton in the final RIXS state in $K_{0.3}MoO_3$ that is not present (or smaller) in α-MoO_3.[9] Such an exciton would have to be small enough to elude detection in XAS measurements.

In conclusion, we have used resonant inelastic x-ray scattering and soft x-ray emission to compare the electronic structure of the metallic quasi-one dimensional Mo bronze $K_{0.3}MoO_3$ with its parent insulator, α-MoO_3. **k**-selective RIXS features were observed in both materials, indicating that the intermediate and final RIXS states in both materials are delocalized. As a consequence of **k**-selectivity, we can place a lower bound on the unoccupied band dispersion in both materials. The unoccupied B* band in α-MoO_3 is calculated to have a ~ 1.5 eV bandwidth,[25] but current $K_{0.3}MoO_3$ calculations assign a bandwidth to the lowest unoccupied band of ~ 0.3 eV [21], underestimating the measured value by a minimum factor of 4/3.

The Boston University (BU) program is supported in part by the Department of Energy under DE-FG02-98ER45680. The BU XES/RIXS spectrometer system was funded by the U.S. Army Research Office under DAAD19-01-1-0364 and DAAH04-95-0014. The experiments at the NSLS are supported by the U.S. Department of Energy, Division of Materials and Chemical Sciences. The ALS is supported by the U.S. Department of Energy under Contract No. DE-AC02-05CH11231. T.L. acknowledges support from the ALS Doctoral Fellowship Program. C.McG. acknowledges financial support from the Irish Higher Educational Authority and Enterprise Ireland.

References:

* Corresponding author. Electronic mail: ksmith@bu.edu

1. K.E. Smith, C. McGuinness, J.E. Downes, P.J. Ryan, S.L. Hulbert, J.M. Honig, and R.G. Egdell, Mater. Res. Soc. Symp. Proc. **755**, DD1.1.1 (2003); K.E. Smith, Solid State Sci. **4**, 359 (2002).

2. A. Kotani and S. Shin, Rev. Mod. Phys. **73**, 203 (2001).

3. S.M. Butorin, J. Elec. Spec. Related Phenom. **110-111**, 213 (2000).

4. L. Perfetti, S. Mitrovic, G. Margaritondo, M. Grioni, L. Forro, L. Degiorgi, and H. Hochst, Phys. Rev. B **66**, 075107 (2002); A.V. Fedorov, S.A. Brazovskii, V.N. Muthukumar, P.D. Johnson, J. Xue, L.C. Duda, K.E. Smith, W.H. McCarroll, M. Greenblatt, and S.L. Hulbert, J. Phys. - Cond. Matter **12**, L191 (2000).

5. C. Schlenker, J. Dumas, C. Escribe-Filippini, H. Guyot, J. Marcus, and G. Fourcaudot, Philos. Mag. B **52**, 643 (1985).

6. M. Greenblatt, Chem. Rev. **88**, 31 (1988).

7. **Low Dimensional Electronic Properties of Molybdenum Bronzes and Oxides**, edited by C. Schlenker (Kluwer Academic Publishers, Dordrecht, 1989), p. Pages.

8. L.C. Duda, J.H. Guo, J. Nordgren, C.B. Stagarescu, K.E. Smith, W. McCarroll, K. Ramanujachary, and M. Greenblatt, Phys. Rev. B **56**, 1284 (1997).

9. Y. Ma, Phys. Rev. B **49**, 5799 (1994).

10. Y. Ma, N. Wassdahl, P. Skytt, J. Guo, J. Nordgren, P.D. Johnson, J.E. Rubensson, T. Boske, W. Eberhardt, and S.D. Kevan, Phys. Rev. Lett. **69**, 2598 (1992); J.A. Carlisle, S.R. Blankenship, L.J. Terminello, J.J. Jia, T.A. Callcott, D.L. Ederer, R.C.C. Perera, and F.J. Himpsel, J. Elec. Spec. Related Phenom. **110**, 323 (2000).

11. J.A. Carlisle, E.L. Shirley, E.A. Hudson, L.J. Terminello, T.A. Callcott, J.J. Jia, D.L. Ederer, R.C.C. Perera, and F.J. Himpsel, Phys. Rev. Lett. **74**, 1234 (1995).

12. S. Eisebitt and W. Eberhardt, J. Elec. Spec. Related Phenom. **110-111**, 335 (2000).

13. P.A. Brühwiler, P. Kuiper, O. Eriksson, R. Ahuja, and S. Svensson, Phys. Rev. Lett. **76**, 1761 (1996); J.A. Carlisle, E.L. Shirley, E.A. Hudson, L.J. Terminello, T.A. Callcott, J.J. Jia, D.L. Ederer, R.C.C. Perera, and F.J. Himpsel, Phys. Rev. Lett. **76**, 1762 (1996).

14. F.M.F. Degroot, M. Grioni, J.C. Fuggle, J. Ghijsen, G.A. Sawatzky, and H. Petersen, Phys. Rev. B **40**, 5715 (1989).

15. J. Nordgren and J.H. Guo, J. Elec. Spec. Related Phenom. **110**, 1 (2000); J. Nordgren and R. Nyholm, Nucl. Instrum. Meth. A **246**, 242 (1986).

16. K. Breuer, K.E. Smith, M. Greenblatt, W. McCarroll, and S.L. Hulbert, J. Phys. Chem. Solids **57**, 1803 (1996); K. Breuer, K.E. Smith, M. Greenblatt, and W. McCarroll, J. Vac. Sci. Technol. A **12**, 2196 (1994).

17. K. Breuer, D.M. Goldberg, K.E. Smith, M. Greenblatt, and W. McCarroll, Solid State Comm. **94**, 601 (1995).

18. J. Graham and A.D. Wadsley, Acta Cryst. **20**, 93 (1966).

19. G.K. Wertheim, L.F. Schneemeyer, and D.N.E. Buchanan, Phys. Rev. B **32**, 3568 (1985).

20. M. Sing, R. Neudert, H. von Lips, M.S. Golden, M. Knupfer, J. Fink, R. Claessen, J. Mucke, H. Schmitt, S. Hufner, B. Lommel, W. Aβmus, C. Jung, and C. Hellwig, Phys. Rev. B **60**, 8559 (1999).

21. J.L. Mozos, P. Ordejon, and E. Canadell, Phys. Rev. B **65**, 233105 (2002).

22. F. Gel'mukhanov and H. Agren, Phys. Rep. **312**, 91 (1999).

23. H.M. Tsai, K. Asokan, C.W. Pao, J.W. Chiou, C.H. Du, W.F. Pong, M.H. Tsai, and L.Y. Jang, Appl. Phys. Lett. **91** (2007).

24. T. Learmonth, C. McGuinness, P.A. Glans, B. Kennedy, J. St.John, J.H. Guo, M. Greenblatt, and K.E. Smith, Phys. Rev. B **(*submitted*)** (2008).

25. A.D. Sayede, T. Amriou, M. Pernisek, B. Khelifa, and C. Mathieu, Chem. Phys. **316**, 72 (2005).

26. C.A. Rozzi, F. Manghi, and F. Parmigiani, Phys. Rev. B **68**, 075106 (2003).

Figure Captions

Figure 1: The crystal structure of $K_{0.3}MoO_3$, and α-MoO_3. Panel (a) shows the conducting **b** axis of $K_{0.3}MoO_3$ projected into the page. The solid parallelogram is the $K_{0.3}MoO_3$ unit cell. Clusters of six MoO_6 octahedra form logical units which are repeated, one of which is enclosed in a dashed box. These clusters are corner sharing along the approximate [102] axis to form sheets with K sites in between. Panel (b) shows one of the $K_{0.3}MoO_3$ logical units rotated 90< about the [102] axis, revealing a chain structure along the **b** axis with both edge and corner sharing octahedra. Panel (c) shows α-MoO_3 with the chain axis projected into the page. The solid rectangle is the unit cell. Here pairs of MoO_6 octahedra form the repeated logical units, with one enclosed in a dashed rectangle. Panel (d) shows one of the α-MoO_3 logical units rotated 90< about the **a** axis, revealing a double chain along the **b** axis.

Figure 2: Top panel: O *K*-edge XES and XAS from $K_{0.3}MoO_3$. $\mathbf{E}_{in} \parallel \mathbf{b}$ (open symbols) and $\mathbf{E}_{in} \parallel$ [102] (solid symbols). Bottom panel: O *K*-edge XES and XAS from α-MoO_3; $\mathbf{E}_{in} \parallel \mathbf{b}$.

Figure 3: RIXS and XAS from $K_{0.3}MoO_3$. Top panel: O *K*-edge XAS. Bottom panel: series of O *K*-edge RIXS spectra as a function of excitation energy. Energies used are marked on the XAS spectrum. All spectra collected with $\mathbf{E}_{in} \parallel \mathbf{b}$.

Figure 4: RIXS and XAS from α-MoO_3. Top panel: O *K*-edge XAS. Bottom panel: series of O *K*-edge RIXS spectra as a function of excitation energy. Energies used are marked on the XAS spectrum. All spectra collected with $\mathbf{E}_{in} \parallel \mathbf{b}$.

Figure 5: Dependence of the energy of the RIXS features in $K_{0.3}MoO_3$ and α-MoO_3 on excitation energy. In the bottom panel, the emission energies of features *i* and *ii* in both materials are plotted against the excitation energy. In the top panel, the excitation energy of each RIXS spectrum represented is plotted. The excitation energy scales for the two materials are shifted such that the lowest excitation energies are aligned. The resulting plot, in the completely non-interacting picture, is a RIXS bandmap of $K_{0.3}MoO_3$ and α-MoO_3, with the lowest unoccupied band in the top panel, and the two observed occupied bands in the bottom panel. In this picture the excitation energy axis can be viewed as a momentum axis, and the feature energy axis as a binding energy axis. The similarity between the two materials is apparent.

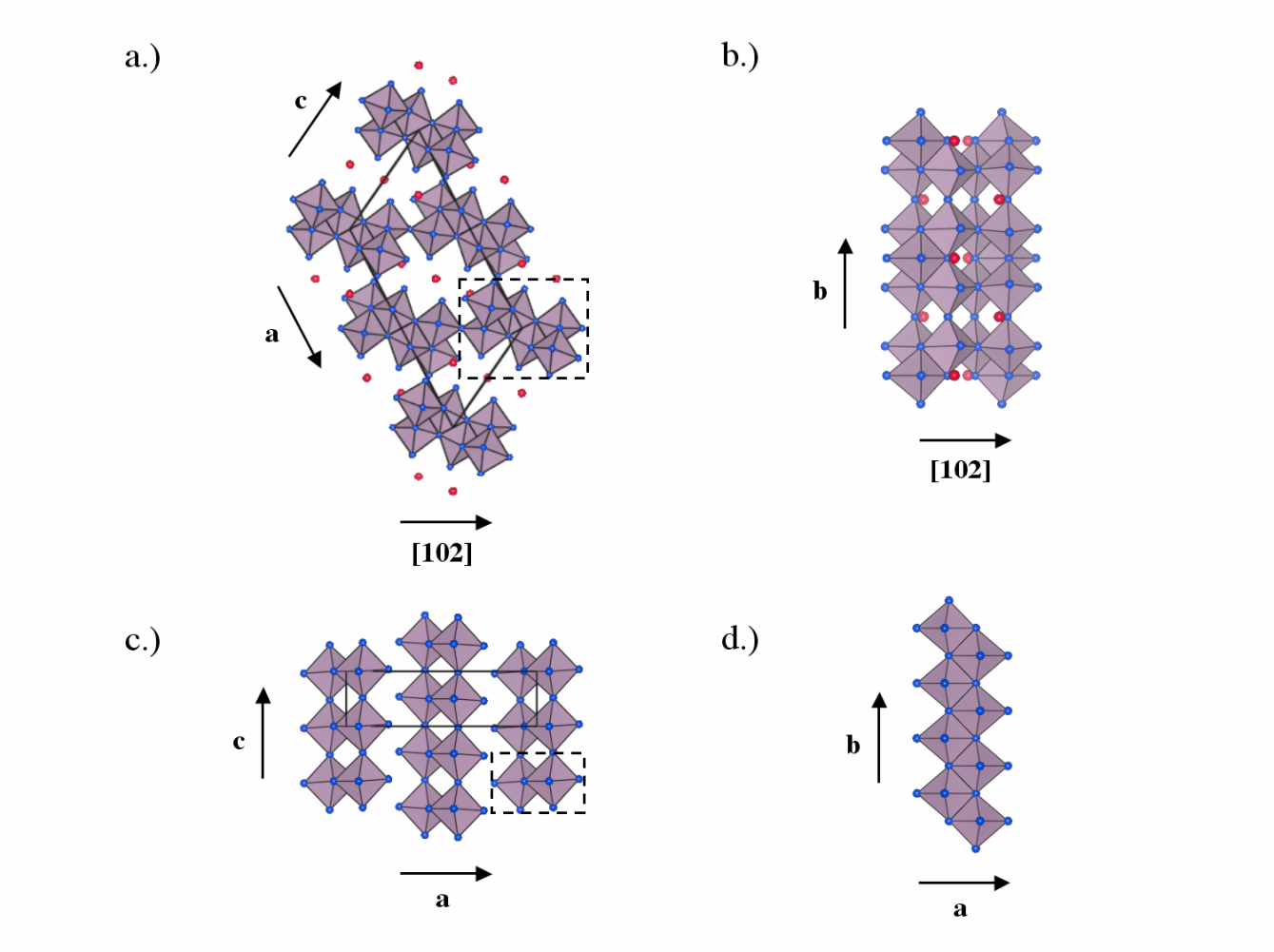

Fig. 1

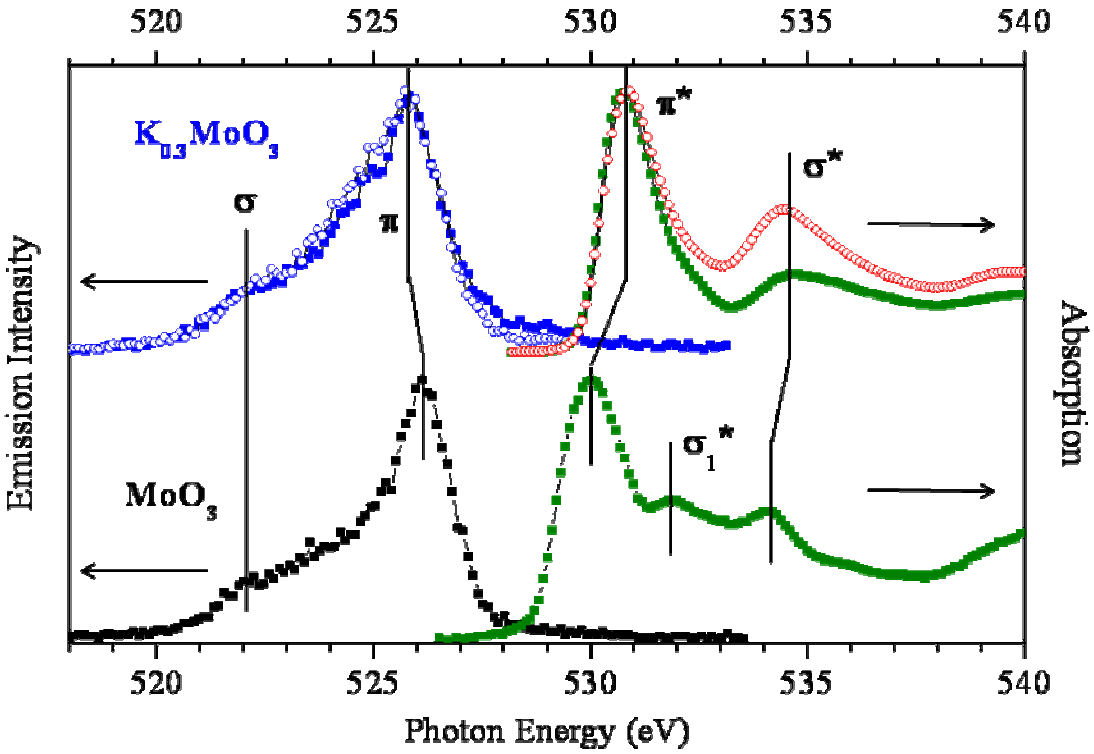
520
525
530
535
540
$K_{0.3}MoO_3$
σ
π
π*
σ*
MoO_3
σ_1*
Emission Intensity
Absorption
Photon Energy (eV)

Fig. 2

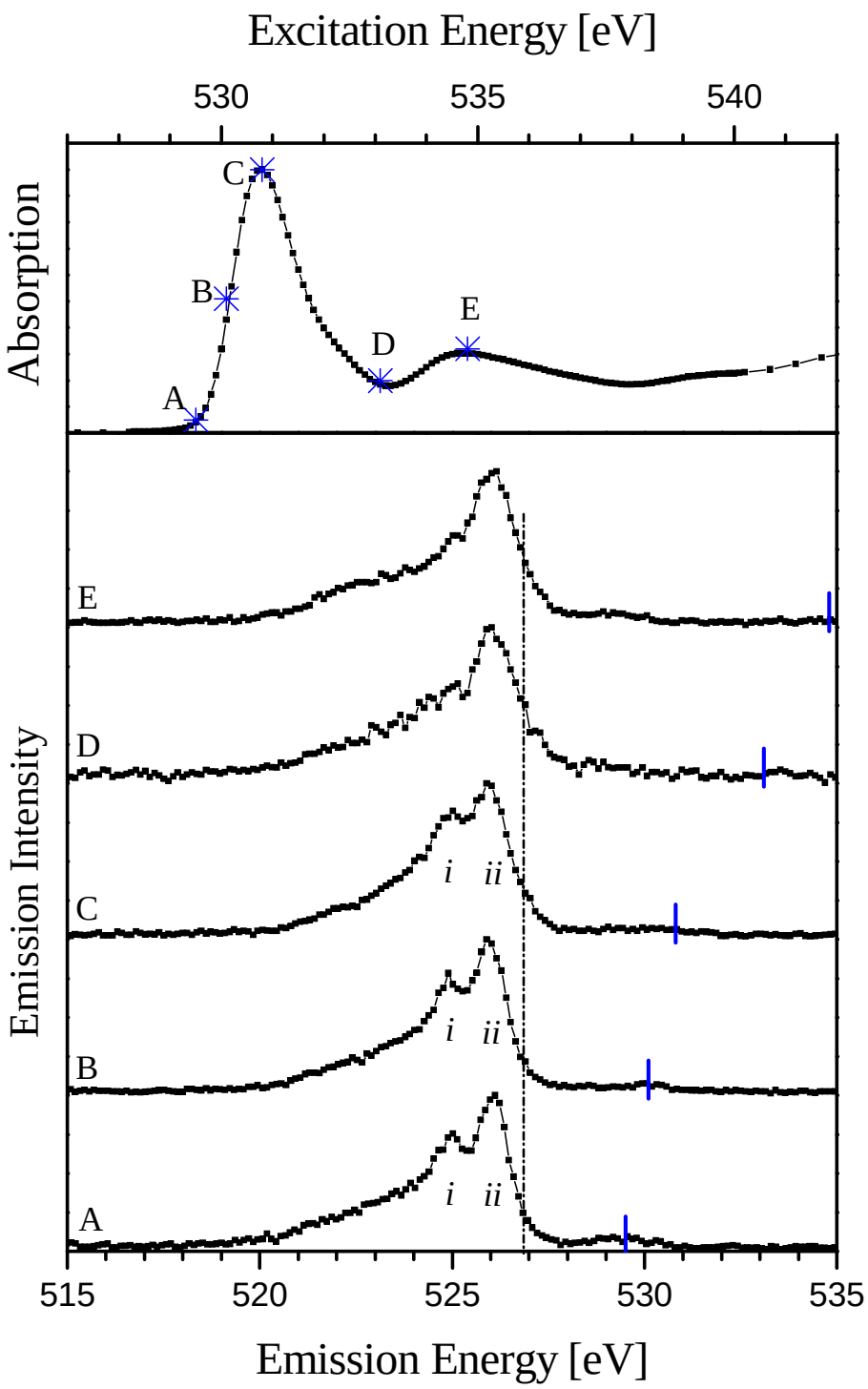
Excitation Energy [eV]
530
535
540
Absorption
A
B
C
D
E
Emission Intensity
E
D
C
B
A
i
ii
515
520
525
530
535
Emission Energy [eV]

Fig. 3

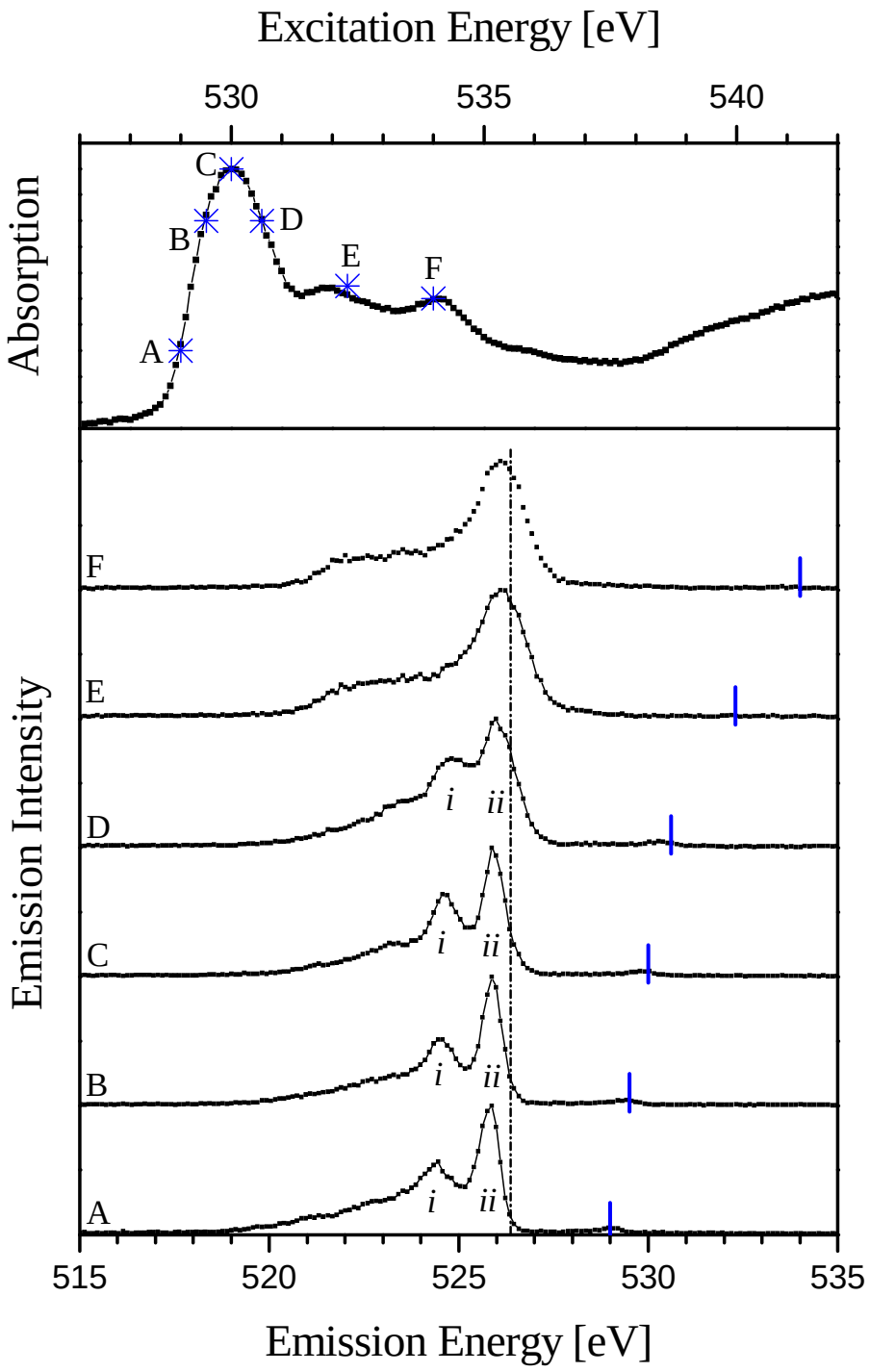
Excitation Energy [eV]
530
535
540
Absorption
A
B
C
D
E
F
Emission Intensity
F
E
D
C
B
A
i
ii
515
520
525
530
535
Emission Energy [eV]

Fig. 4

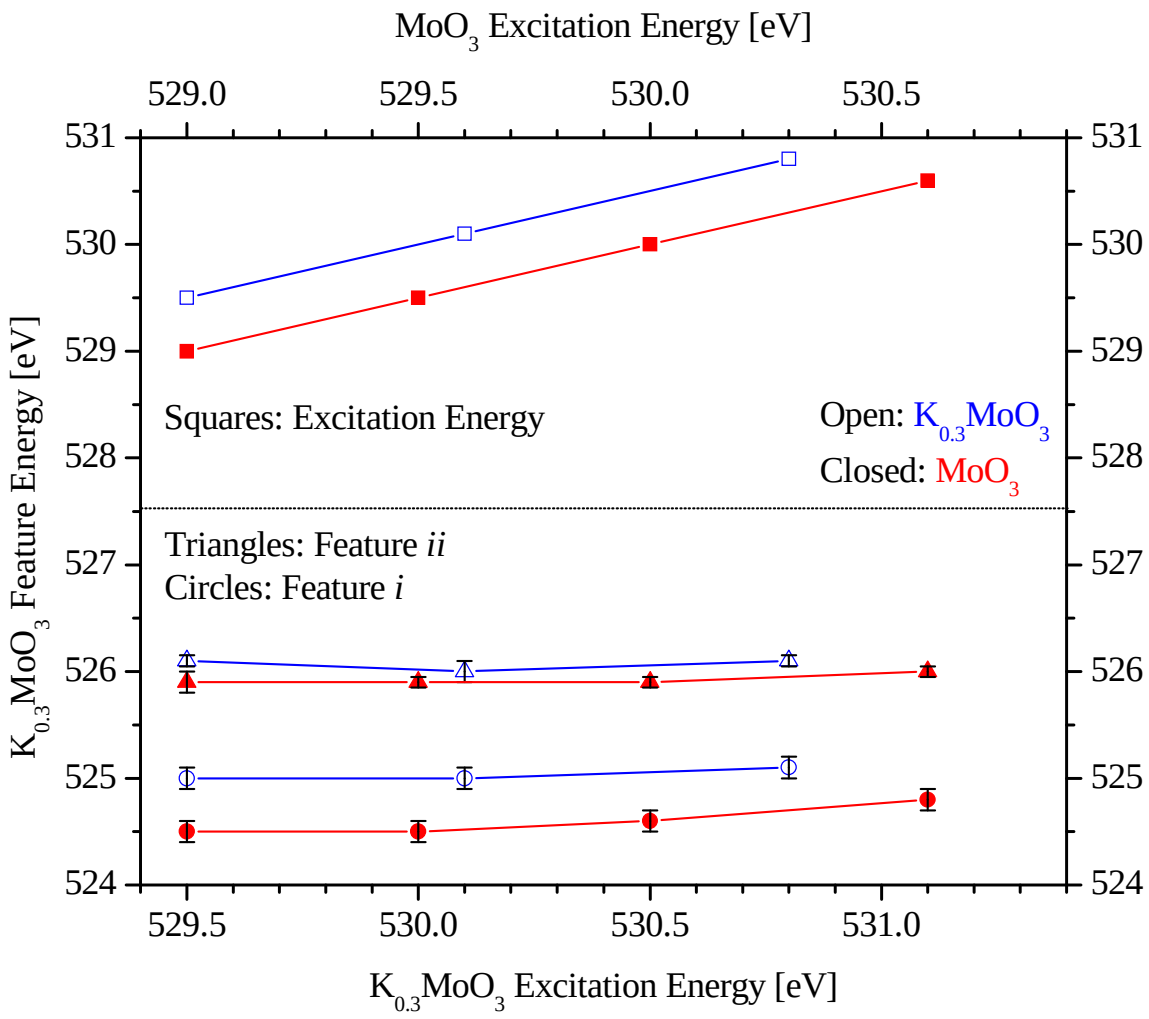
MoO3 Excitation Energy [eV]
529.0
529.5
530.0
530.5
531
530
529
528
527
526
525
524
K0.3MoO3 Feature Energy [eV]
Squares: Excitation Energy
Open: K0.3MoO3
Closed: MoO3
Triangles: Feature ii
Circles: Feature i
529.5
530.0
530.5
531.0
K0.3MoO3 Excitation Energy [eV]

Fig. 5